Cerebral Cortex July 2011;21:1602–1612
doi:10.1093/cercor/bhq225
Advance Access publication November 17, 2010

Contributions of the PPC to Online Control of Visually Guided Reaching Movements Assessed with fMRI-Guided TMS

Alexandra Reichenbach[1,2], Jean-Pierre Bresciani[1,3], Angelika Peer[4], Heinrich H. Bülthoff[1,5] and Axel Thielscher[2]

[1]Department of Human Perception, Cognition and Action, Max Planck Institute for Biological Cybernetics, 72076 Tübingen, Germany, [2]Department of High-Field Magnetic Resonance, Max Planck Institute for Biological Cybernetics, 72076 Tübingen, Germany, [3]Laboratory of Psychology and NeuroCognition, UMR CNRS 5105 Université Pierre-Mendès-France, 38040 Grenoble, France, [4]Institute of Automatic Control Engineering, Technische Universität München, 80290 München, Germany and [5]Department of Brain and Cognitive Engineering, Korea University, 136-701 Seoul, Korea

Address correspondence to A. Reichenbach, Department of High-Field Magnetic Resonance, Department of Human Perception, Cognition and Action, Max Planck Institute for Biological Cybernetics, Spemannstrasse 41, 72076 Tübingen, Germany. Email: alexandra.reichenbach@tuebingen.mpg.de.

The posterior parietal cortex (PPC) plays an important role in controlling voluntary movements by continuously integrating sensory information about body state and the environment. We tested which subregions of the PPC contribute to the processing of target- and body-related visual information while reaching for an object, using a reaching paradigm with 2 types of visual perturbation: displacement of the visual target and displacement of the visual feedback about the hand position. Initially, functional magnetic resonance imaging (fMRI) was used to localize putative target areas involved in online corrections of movements in response to perturbations. The causal contribution of these areas to online correction was tested in subsequent neuronavigated transcranial magnetic stimulation (TMS) experiments. Robust TMS effects occurred at distinct anatomical sites along the anterior intraparietal sulcus (aIPS) and the anterior part of the supramarginal gyrus for both perturbations. TMS over neighboring sites did not affect online control. Our results support the hypothesis that the aIPS is more generally involved in visually guided control of movements, independent of body effectors and nature of the visual information. Furthermore, they suggest that the human network of PPC subregions controlling goal-directed visuomotor processes extends more inferiorly than previously thought. Our results also point toward a good spatial specificity of the TMS effects.

Keywords: functional magnetic resonance imaging localizer, motor control, online responses, posterior parietal cortex, transcranial magnetic stimulation

Introduction

Every day, humans reach for objects in the environment with an incredible high degree of precision. Such behavior is seemingly effortless, even when sudden perturbations such as object relocations occur (Prablanc and Martin 1992; Pisella et al. 2000). This skill necessitates the fast processing of sensory information about our body and the environment in order to continuously control our movement (Desmurget and Grafton 2000). The sensory information available is usually composed of visual information about the object to reach for (called external visual information in the following), visual information about the body's effectors (called body-related visual information in the following), and proprioceptive information about the body's effectors.

The brain regions integrating information from different sensory channels for motor control have been investigated in humans using functional magnetic resonance imaging (fMRI) and transcranial magnetic stimulation (TMS; for reviews, see Culham and Valyear 2006; Iacoboni 2006; Filimon 2010). Although there is agreement that the posterior parietal cortex (PPC) contributes to many processes for online control of reaching movements, like coordinate transformations, the reported subregions vary substantially between studies. This might be due, on the one hand, to the wide variety of tasks used in the different studies and on the other hand to the high interindividual variance in neuroanatomy within the PPC (Grefkes and Fink 2005). Therefore, a consensus on the functional neuroanatomy of the human PPC in motor control is still missing. While studies on nonhuman primates deliver a more clear-cut view on this topic, applying this knowledge to humans remains a challenge, as pointed out by recent comparative work (Culham and Kanwisher 2001; Grefkes and Fink 2005).

The goal of the present study was to identify subregions of the PPC that contribute to the integration of visual information during online control of reaching movements. In order to distinguish between the processing of external and body-related visual information, 2 types of perturbations were investigated in a reach-to-target paradigm: displacement of the visual target (corresponding to external visual information; Prablanc and Martin 1992) and displacement of the visual feedback of the hand position (corresponding to body-related visual information; Sarlegna et al. 2003). The former perturbation was investigated both with and without visual feedback about the hand position as the "mode" of motor control might differ as a function of the available visual information about the hand (Krakauer et al. 1999; Reichenbach et al. 2009). Consequently, different processes and brain regions might be recruited to some extent. Furthermore, when visual information about the target and proprioceptive information from the body effectors has to be integrated, extra coordinate transformations are necessary to bring this information into a common frame of reference.

In contrast to prior studies (Desmurget et al. 1999; Johnson and Haggard 2005; Chib et al. 2009), we combined an fMRI localizer task with subsequent neuronavigated TMS experiments for the same subjects. The fMRI localizer gave an approximate overview over the areas generally involved in online control during visuomotor processing. This enabled accurate selection of individual TMS stimulation sites. Our approach therefore took into account interindividual

differences in (functional) neuroanatomy of the human PPC. The fMRI localizer yielded a better spatial localization of the TMS results, while TMS allowed us to causally disentangle necessary from coactivated brain areas, thus underpinning the importance of a subset of the areas detected by fMRI.

Materials and Methods

General Procedure

Nine healthy volunteers (aged 23–34 years, 5 females) including 2 of the authors participated in the study. Besides the authors, all subjects were naive to the purpose of the study. They had normal or corrected-to-normal vision and no history of neurological disorders. Written informed consent was obtained for each subject prior to the first experiment. The study was conducted in accordance with the Declaration of Helsinki and approved by the local ethics committee of the Medical Faculty of the University of Tübingen. Each subject participated in several experimental sessions in which he/she was first familiarized with the overall procedure, then the fMRI data were recorded, and finally the different TMS experiments were performed. Successive sessions were separated by 1 week or more. During the MRI scan and the TMS experiments, subjects wore earplugs to prevent hearing damage and auditory influence on task performance. One subject dropped out in the course of the study due to personal reasons unrelated with the experiment.

Two different visual perturbations were applied in order to investigate the subregions of the PPC contributing to the integration of external and body-related visual information during reaching: the displacement of the visual target (abbreviated TD indicating "target displacement," Fig. 1*a*) and the displacement of the visual feedback about the hand position (abbreviated HD indicating "hand displacement," Fig. 1*b*) after onset of the reaching movement.

In the fMRI localizer task, brain regions were identified that were robustly activated during reaching (compared with fixation with matched visual input) and, in addition, were more active during perturbed than during unperturbed reaching (Fig. 2*a–c*). Brain region identification was done separately for TD and HD. These regions, and additionally some control sites, provided the basis for selecting the stimulation sites of the subsequent (causal) TMS experiments. The paradigms for the TMS and fMRI experiments were matched apart from one detail, in order to prevent artifacts in the fMRI images. In the fMRI localizer, we used finger reaching with the tip of the index finger attached to an MR-compatible joystick placed beside the hip and the visual scene projected onto a coil mounted mirror. The TMS experiments were conducted in a virtual reality environment with spatially matched visual and haptic scenes where the subjects had to perform fully fledged reaching movements with their right arm using a robot arm as manipulandum (Supplementary Fig. S1). Importantly, however, the type and extent (in degrees) of the visual perturbations were the same for both imaging modalities.

In the TMS main experiments, we tested whether the subjects' ability to correct for visual perturbations was reduced when magnetic pulses were applied to the brain regions previously identified by fMRI but not when applied to control sites. The first 2 TMS experiments investigated the responses to visual TDs, first with and then without visual feedback about the hand position (TMS experiment 1: TD_HF and TMS experiment 2: TD_nHF, Fig. 1*a*). In the third experiment, the effects of displacing the visual feedback about the hand position were tested (TMS experiment 3: HD, Fig. 1*b*).

Details on the fMRI localizer experiment can be found in the Supplementary Data B. The following paragraphs first describe how the TMS stimulation sites were derived from the fMRI results and then depict the methods of the TMS experiments. The Results section is identically organized.

TMS Stimulation Sites

The peak activations within the regions that exhibited higher blood oxygen level–dependent (BOLD) activity during perturbed than during unperturbed reaching in the fMRI localizer task (Fig. 2*b,c*) were used to determine the TMS stimulation sites. Most TMS stimulation sites were based on group results. The statistical group maps were transformed back from Montreal Neurological Institute (MNI) space to the space of the individual structural images, and the closest coil position on the skull was determined for each activation peak using custom-written MATLAB routines (The MathWorks). The routines used the surface reconstruction of the skull as obtained with BrainVoyager 2000 (Brain Innovation). Additional individual stimulation sites were defined whenever the individual activation peak within a given anatomical region was spatially offset from the corresponding peak in the group map, that is, when planning the coil position based on the individual activation peak resulted in a coil position >10 mm apart from the position planned on the peak of the group activation. In the TMS experiments, these individual sites were tested in addition to the sites derived from the fMRI group activations. An additional level for the factor "stimulation site" was defined for the statistical group analyses whenever an anatomical region included individual stimulation sites: The first level representing a particular region was based solely on the TMS data gathered at the fMRI group site (indicated by the subscript "group" in the following). The additional level was used to represent the individual test sites. It contained the data from the individual sites whenever they existed and the data acquired at the group site for the remaining subjects (indicated by the subscript "indiv" in the following). In each case, data from all 9 subjects (8 subjects for experiment 2) were used to compile the TMS results at the group level.

TMS Experiments: Technical Setup

A mirror-setup with a top-mounted CRT monitor and shutter glasses (StereoGraphics/REAL D) was used to render the 3D visual scene in spatial congruence to the haptic scene (Supplementary Fig. S1). The latter was controlled by a robot arm (DekiFeD, Technische Universität München, Germany; Buss and Schmidt 1999) used as manipulandum that restricted the hand movements to a horizontal plane. The subjects kept the handle that was mounted on the robot arm grasped with the right-hand throughout an experimental block, and the visual feedback about the hand position (represented by a red sphere), whenever given, corresponded spatially to the top of this handle. The robot arm actively followed the hand movements to minimize its inertia as felt by the subject. Visual scene presentation and acquisition of the kinematic data were performed at 120 Hz. For additional details, please refer to Reichenbach et al. (2009).

Saccade detection was realized online via electrooculography (EOG) on a separate computer. Three small cup electrodes were placed on the subject's face, above and below the right eye, and the reference in the center of the forehead. The electrodes were connected to the AD-converter (DAQ2205; Adlink Technology Inc., sampling rate 10 kHz) of the computer via an amplifier (Psylab, Contact Precision Instruments Inc.). A custom-written MATLAB program reported the saccades to the computer that controlled the experiment. The EOG threshold was adjusted for each subject so that the saccade triggers corresponded to the initial acceleration period of the eye movement.

Biphasic TMS stimuli were applied using a Medtronic MagPro X100 stimulator (MagVenture) with a MC-B70 butterfly coil. The coil position was monitored using a neuronavigation system (BrainView, Fraunhofer IPA; for a description of the system, see Kammer et al. (2007)). The spatial accuracy of the registration between the subject's real head and his anatomical MR image in the neuronavigation system was established at the beginning and checked again at the end of each session using the positions of clearly visible landmarks (e.g., nasion and inion). The coil was held manually by a trained investigator, keeping the coil position in a range of 2 mm to the preplanned stimulation sites. Blocks were repeated whenever the distance of the coil to the stimulation site exceeded 2 mm. The stimulation intensity was chosen to meet 2 competing goals: It should be as high as possible to maximize the impact on the stimulation site without eliciting direct effects on M1. For this purpose, the coil was placed at the most anterior stimulation site at the beginning of each session, and the intensity was gradually decreased until no motor responses were elicited in the finger muscles any more for at least 10 consecutive trials (tested by recording surface electromyography from the relaxed first dorsal interosseus). Subsequent control measurements confirmed that this procedure resulted

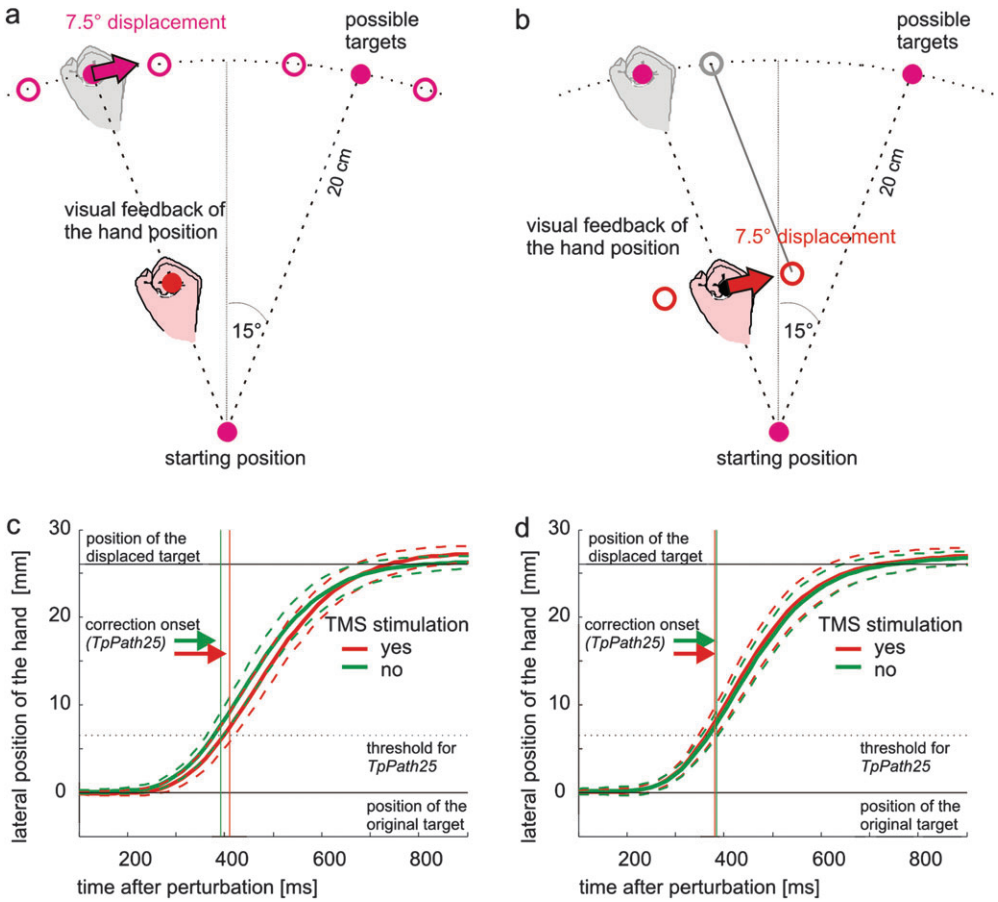

Figure 1. Upper panel: schematic sketch of the arrangement of the visual scene for both the fMRI and the TMS experiments. The locations of the starting position and of the visual targets are shown as filled magenta circles. The grayed out components illustrate the scenario at the end of the perturbed movements if the subject had not corrected for the corresponding perturbation. All perturbations required an amendment of the hand by 7.5° (rotated relative to the starting circle) from the original target direction at the end of the reaching movement. (*a*) The spatial displacements of the visual target (TD) are depicted as open circles (fMRI condition 2 and TMS experiments 1 and 2). (*b*) The open circles indicate the displacements of the visual feedback about the hand position (HD) (fMRI condition 3 and TMS experiment 3). Lower panel: mean kinematic data (dashed lines: SE across subjects) for illustration of TpPath25 for IPS_{group} (*c*) and reach (*d*) for the first TMS experiment (TD_HF). Data of all perturbed conditions are collapsed and only the lateral position of the hand (i.e., the component perpendicular to the original reaching direction) is plotted against time. As long as the hand is heading straight to the original target, no lateral displacement is visible on the *y*-axis. The displacement of 7.5° in a distance of 20 cm corresponds to a lateral displacement of 26.1 mm. Corresponding spatial 2D trajectories can be found in the Supplementary Data (Supplementary Fig. S2).

in a stimulation intensity of ~90% relative to the individual motor threshold. Finger muscles were used for this purpose as it is known that these muscles exhibit the lowest TMS thresholds. The coil was initially oriented parallel to the central sulcus and adjusted when necessary. This procedure resulted in stimulation intensities of 48–61% of maximum stimulator output.

TMS Experiments: Procedure and Behavioral Task

In separate sessions, 3 different visual conditions were tested: displacement of the visual target, first with and then without visual feedback about the hand position (TMS experiment 1: TD_HF and TMS experiment 2: TD_nHF, Fig. 1*a*), and displacement of the visual feedback about the hand position (TMS experiment 3: HD, Fig. 1*b*). The independent variables tested that were common to all 3 experiments were position of the target (15° to the left/15° to the right), visual perturbation (7.5° to the right/7.5° to the left/none), and TMS (yes/no). The number of trials without TMS was equated to the number of TMS trials. The timing between the initial saccade to the visual target and the magnetic pulses (called TMS stimulus onset asynchrony (SOA) in the following) was 40 ms. For experiment 2 (TD_nHF), an additional later TMS SOA of 80 ms was used, resulting in 3 levels for the variable TMS in this case (80 ms/40 ms/no). The additional TMS SOA was based on results from a prior psychophysical study (Reichenbach et al. 2009) which indicated that online corrections to displaced targets are slower when visual feedback about the hand position was not available.

A session proceeded in complete darkness and consisted of several blocks, including an initial training block to familiarize the subject with the task. One block lasted 10–15 min and contained 72 trials, covering all possible combinations of the independent variables. The order of presentation was fully randomized to prevent any predictability or anticipation of the visual perturbation and the administration of TMS. Altogether, 12 repetitions were recorded for each combination of independent variables, resulting in 2 (TMS experiments 1 and 3) or 4 (TMS experiment 2) blocks per TMS stimulation site. The order of stimulation sites was randomized to prevent training or fatigue effects from biasing the results. With exception of the right hemispheric control site, the stimulation positions were undistinguishable for the subjects. Depending on the experiment and the subject (having individual test sites or not), the number of stimulation sites varied between 3 and 8. The highest number of sites was tested for TD_HF so that some of the control sites were tested in a separate session for this visual condition.

A trial started with the presentation of the starting position with the visual feedback about the hand position present. The starting position was randomly jittered in a 2 × 2 cm area located 10 cm in front of the subject about the body midline. After the hand had been maintained in the starting position for about 1 s, the target appeared and the starting position disappeared. The target was displayed at 20 cm distance from

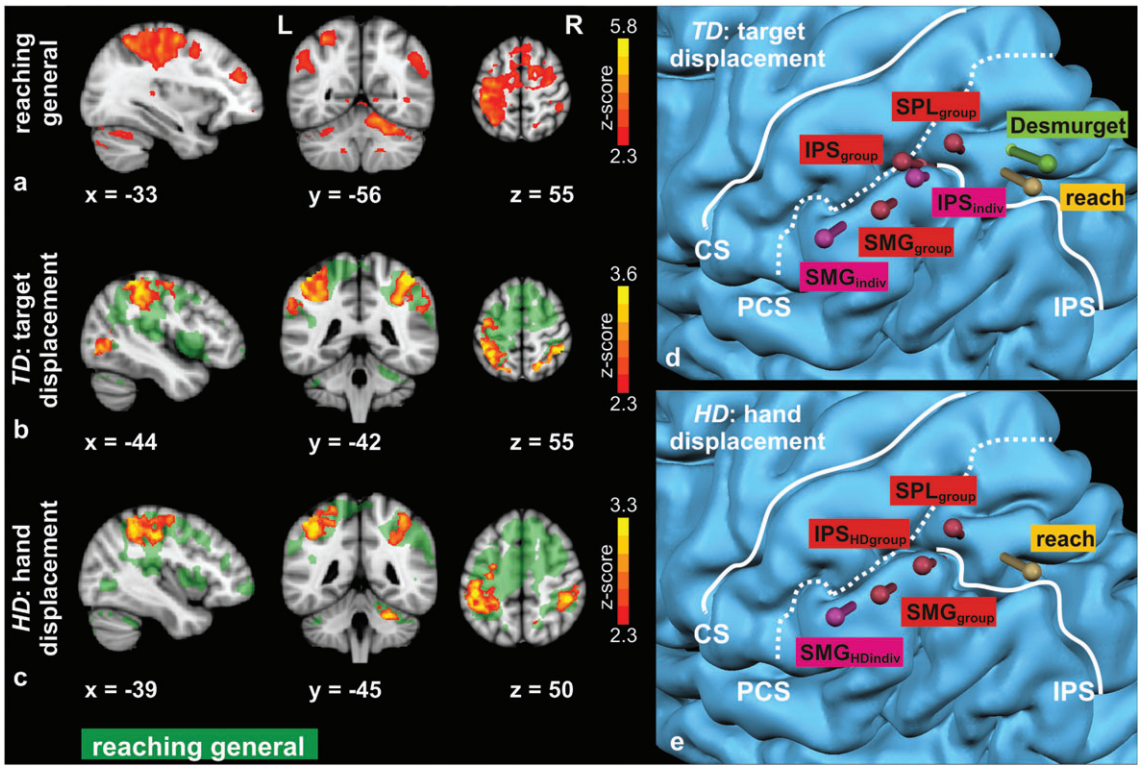

Figure 2. Left panel: fMRI activation patterns for the group analysis (all maps were thresholded using $Z = 2.3$ at voxel level and $P = 0.05$ corrected at cluster level; MNI space). The entire fMRI experiment was conducted with visual feedback about the cursor position present. (*a*) Activation pattern for general reaching compared with fixation. The depicted slices were selected using the MNI coordinates of the local peak activation in the left PPC. This contrast was used as mask for the subsequent fMRI analyses. (*b*) Activation pattern for displacement of the visual target (TD) compared with unperturbed reaching. The depicted slices were selected according to the position of the absolute peak activation, the latter residing within the left PPC. This activation map served as basis for planning the stimulation sites of TMS experiments 1 and 2 (Fig. 2*d*). (*c*) Activation pattern for displacement of the visual feedback of the "hand" position, that is, the cursor position on the screen (HD) compared with unperturbed reaching. The slices were selected according to the local peak activation in the left PPC. This activation map was used to plan the stimulation sites of TMS experiment 3 (Fig. 2*e*). Right panel: (*d*) stimulation sites for TMS experiments 1 and 2 with displacement of the visual target (TD) as derived from the fMRI activations. (*e*) Stimulation sites for TMS experiment 3 with displacement of the visual feedback about the hand position (HD). The MNI group coordinates were transformed in one subject's individual space and then projected onto the rendered 3D reconstruction of this subjects' left hemisphere. The "needles" indicate the different coil positions: Their direction is aligned perpendicular to the TMS coil and their head is located directly at the center of the coil on the skull. The white lines highlight the principle sulci: central sulcus (CS), postcentral sulcus (PCS), IPS.

the starting position, and its location was 15° on either side of the body midline. The subject's task was to look at and reach for the target as quickly and precisely as possible. In experiment 2 (TD_nHF), the visual feedback about the hand position disappeared as soon as the target appeared. The time at which the velocity of the hand dropped below 1 cm/s again was defined as the end of the trial. In between trials, the visual scene disappeared for 2 s.

Visual perturbations were set to occur while the subject performed the saccade to the target to prevent them being consciously perceived (Zuber and Stark 1966). In the first 2 experiments (TD_HF and TD_nHF), the visual target was displaced 7.5° on either side of its original location (Fig. 1*a*). In the third experiment (HD), the visual feedback about the hand position was translated perpendicular to the original reaching direction on either side of its original location to yield in an offset of 7.5° at the end of the movement (Fig. 1*b*).

In TMS trials, 3 magnetic pulses were applied at a frequency of 60 Hz. The first pulse was delivered at a fixed delay of 40 ms (or 80 ms for the later SOA in experiment 2) with respect to the time of the visual perturbation (i.e., after the saccade). The 3 pulses of the 40 ms SOA covered a period of 33 ms after hand movement onset (Desmurget et al. 1999).

In order for participants to remain naive throughout the complete duration of the study, no explicit questions about the subject's awareness of the applied perturbations were asked. Instead, after each session, the subjects were encouraged to disclose any oddity they encountered during the course of the experiment. Some subjects reported that sometimes it "felt weird" or about "being worse than expected" but all clearly missed the real reason for it.

TMS Experiments: Behavioral Measures and Data Analysis

The onset and offset of the movement were defined as the time at which the velocity of the robot arm exceeded and fell below 2 cm/s, respectively. Trials were excluded from further analysis if total time, total path length, or peak velocity were outside the range of the subject's mean ± 3 × standard deviation. The impact of TMS on the online corrections to the visual perturbations was assessed by applying 2 different measures to the kinematic data. The time point at which the mean trajectory first exceeded 25% of the distance necessary to fully compensate for the perturbation was used as temporal measure of the correction onset (TpPath25; Fig. 1*c*,*d*; Reichenbach et al. 2009). The absolute value of the maximum deviation between the recorded trajectory and an "ideal trajectory" (i.e., a straight line between the starting position and the final target) was used as the spatial measure for the amount of incorrect reaching (MaxDev). Additionally, measurements of the overall reaching time (ReachTime) and endpoint accuracy (EndAcc) were assessed. The latter was defined as the distance of the final hand position to the final target, whereby the evaluation was restricted to the component perpendicular to the original reaching direction (a displacement of 7.5° in the distance of 20 cm yields in a lateral displacement of 26.1 mm). Group analyses for each TMS experiment were conducted with repeated-measures analyses of variance (ANOVAs) on the factors TMS (TMS SOA(s)/TMS not applied) and stimulation site. Subsequently, for each stimulation site, preplanned comparisons between each TMS SOA versus TMS not applied were conducted. Fisher's least significant difference tests were used for multiple comparisons correction when the interaction of the ANOVA was

significant. Reported values are mean ± standard error (SE) across subjects, unless stated otherwise.

Results

TMS Stimulation Sites: Results of the fMRI Localizer Task

General reaching-related activity compared with fixation mainly clustered in the left hemisphere (Fig. 2*a*), spanning from motor cortex over somatosensory cortex to the PPC. Additional strong activations occurred bilaterally in the frontal lobes (including premotor areas) and the right cerebellum. A smaller cluster was present in the right PPC. The peak activation within the left PPC was used to plan a TMS control site ("reach"; see Tables 1–3 for the MNI coordinates on which all stimulation sites are based upon). Evaluation of the behavioral data confirmed that the subjects corrected for the visual perturbations, even though the overall movements were small (data not shown).

The stimulation sites for TMS experiment 1 (TD_HF; Fig. 2*d*) were based on the comparison of reaching trials with displacement of the visual target (TD) versus unperturbed trials (Fig. 2*b*). A large left-lateralized cluster exhibited enhanced BOLD activity during perturbed versus unperturbed reaching. The peak difference was observed in the anterior part of the intraparietal sulcus (resulting in stimulation site IPS_{group}) and additional local peaks occurred on the anterior supramarginal gyrus (aSMG) and the anterior superior parietal lobe (resulting in sites SMG_{group} and SPL_{group}). Additionally, 3 subjects had robust individual peaks more posteriorly within the IPS (resulting in individual TMS stimulation sites displaced by 11–17 mm from IPS_{group}), and 5 subjects had robust individual peaks more inferiorly on the SMG (resulting in individual TMS stimulation sites having a distance of 19–39 mm to SMG_{group}). These positions were included as additional individual TMS stimulation sites (IPS_{indiv} and SMG_{indiv}). At the group level, the comparison revealed an additional small peak in the right PPC that approximately mirrored the position of IPS_{group} and that was therefore selected as control stimulation site over the right hemisphere (IPS_{right}). One additional test site was obtained using the procedure of Desmurget et al. (1999), independent of the fMRI localizer results. For TMS experiment 2 (TD_nHF), which served as an addendum to test whether the observed TMS effects (as described below) depended on visual feedback about the hand position, we used a subset of these sites (IPS_{indiv}, SMG_{indiv}, and SPL_{group}).

The sites for TMS experiment 3 (HD; Fig. 2*e*) were based on regions that exhibited enhanced BOLD activity for reaching trials with displacement of the visual feedback about the hand position (HD) versus unperturbed trials (Fig. 2*c*). The peak difference within the PPC was located in the anterior part of the IPS (resulting in site $IPS_{HDgroup}$). Six subjects had robust individual peaks on the inferior SMG (resulting in individual TMS stimulation sites 11–33 mm distant to SMG_{group}) that were used as additional stimulation sites ($SMG_{HDindiv}$). At the group level, a peak was present in the right IPS that served as control site over the right hemisphere ($IPS_{HDright}$). Positions SMG_{group} (situated between $IPS_{HDgroup}$ and $SMG_{HDindiv}$) and SPL_{group} were included as additional test sites in order to cover the complete region ranging from SMG to SPL comparable with the preceding 2 experiments. At both positions, BOLD activity for HD trials was clearly enhanced compared with unperturbed reaching, even though it did not peak there.

TMS Experiment 1: Displacement of the Visual Target with Visual Feedback of the Hand Position (TD_HF)

For trials with displacement of the visual target, overall reaching times were selectively prolonged by TMS stimulation over sites IPS_{group}, SMG_{group}, and SMG_{indiv} (ReachTime in Table 1; interaction TMS × stimulation site: $F_{7,56} = 3.77$; $P < 0.01$). Endpoint accuracy was generally good and not affected by TMS stimulation (EndAcc in Table 4). The online correction for the perturbation started significantly later when TMS was applied over sites IPS_{group}, IPS_{indiv}, and SMG_{indiv} (TpPath25 in Table 1; interaction TMS × stimulation site: $F_{7,56} = 2.85$; $P < 0.05$). Accordingly, the maximum deviation was enhanced when TMS was applied over these sites (MaxDev in Table 1; interaction TMS × stimulation site: $F_{7,56} = 2.21$; $P < 0.05$).

Including test sites based on individual fMRI data shifted the mean position of the IPS stimulation site only 4 mm posteriorly. Accordingly, the TMS effects were comparable in both cases (IPS_{indiv} vs. IPS_{group} in Table 1). In contrast, the inclusion of individual sites shifted the mean stimulation site over the SMG 12 mm lateral-inferiorly and resulted in markedly more stable TMS effects (SMG_{indiv} vs. SMG_{group} in Table 1). As the usage of individual sites tended to stabilize the TMS effects, we used IPS_{indiv} and SMG_{indiv} rather than the corresponding group sites in TMS experiment 2.

TMS Experiment 2: Displacement of the Visual Target without Visual Feedback of the Hand Position (TD_nHF)

Compared with the preceding experiment, reaching times were generally slightly shorter (4 ms, Table 4) but were not affected by TMS at any of the 3 stimulation sites (Table 4; main effect of TMS on ReachTime: $P > 0.5$; interaction TMS × stimulation site: $P > 0.05$). The spatial accuracy of the reaching movements was reduced compared with the preceding experiment, as reflected by larger SEs for EndAcc (Table 4).

When separately analyzing the data for the TMS SOAs 40 and 80 ms, the results revealed a tendency toward later correction onsets and enhanced maximum deviation for stimulation sites IPS_{indiv} and SMG_{indiv} compared with SPL_{group} (data not shown). This pattern is similar to the data obtained with visual feedback about the hand position. However, they did not reach statistical significance due to the generally large variability of the movements. We therefore pooled the 2 TMS SOAs in each subject before performing the group analysis. For site SMG_{indiv}, this helped to confirm longer general reaching times (ReachTime in Table 2; interaction TMS × stimulation site: $F_{2,14} = 3.56$; $P = 0.05$) and a later correction onset (TpPath25 in Table 2; interaction TMS × stimulation site: $F_{2,14} = 3.69$; $P = 0.05$) for trials with versus without TMS. The endpoint accuracy was selectively affected by TMS over site IPS_{indiv} (EndAcc in Table 2; interaction TMS × stimulation site: $F_{2,14} = 4.82$; $P < 0.05$).

TMS Experiment 3: Displacement of the Visual Feedback of the Hand Position (HD)

For trials where the visual feedback about the hand position was displaced, the overall reaching time was selectively prolonged by TMS stimulation over sites SMG_{group} and $SMG_{HDindiv}$ (Table 3). As expected from the results of prior studies (Sarlegna et al. 2003, 2004), the correction for the visual perturbation was generally incomplete due to some remaining proprioceptive influence, resulting in negative values for EndAcc (Table 4). This general tendency was not affected by

Table 1
Results for TMS experiment 1 (TD_HF)

Stimulation site	MNI coordinates, *x*, *y*, *z* in [mm], (±SD)	TpPath25, [ms], (*P* values)	MaxDev, [mm], (*P* values)	ReachTime, [ms], (*P* values)	EndAcc, [mm], (*P* values)
SPL_{group}	−36, −49, 57	9.4 ± 6.5	0.6 ± 0.5	−1.3 ± 5.3	−0.6 ± 0.3
IPS_{group}	−44, −42, 55	**18.0 ± 7.9, (<0.01)**	**0.8 ± 0.4, (<0.05)**	**26.3 ± 16.5, (<0.01)**	0.9 ± 0.6
IPS_{indiv}	−42.9/−45.0/52.9, (±1.9 4.7 4.3)	**13.2 ± 6.5, (<0.05)**	**0.7 ± 0.3, (<0.05)**	16.2 ± 15.4	0.1 ± 0.4
SMG_{group}	−45, −40, 45	9.5 ± 4.8	0.1 ± 0.2	**46.0 ± 9.7, (<0.001)**	0.6 ± 0.5
SMG_{indiv}	−53.4, −32.5, 40.3, (±8.3 7.5 5.2)	**19.3 ± 8.3, (<0.01)**	**0.8 ± 0.4, (<0.05)**	**36.0 ± 7.8, (<0.001)**	0.4 ± 0.4
IPS_{right}	44, −42, 57	−3.2 ± 4.4	−0.2 ± 0.3	2.8 ± 8.4	0.1 ± 0.4
Reach	−33, −56, 55	−3.4 ± 5.6	−0.2 ± 0.4	−3.8 ± 4.9	0.4 ± 0.4
Desmurget	−33.9, −59.4, 62.8, (±3.8 3.4 2.3)	−9.9 ± 4.8	−0.5 ± 0.5	5.9 ± 5.6	0.1 ± 0.2

Note: The MNI coordinates upon which the TMS stimulation sites were planned are given and for TpPath25, MaxDev, ReachTime and EndAcc, the difference ± SE between trials with versus without TMS is given for each TMS stimulation site. Statistically significant differences are marked bold.

Table 2
Results for TMS experiment 2 (TD_nHF)

Stimulation Site	MNI coordinates, *x*, *y*, *z* in [mm], (±SD)	TpPath25, [ms], (*P* values)	MaxDev, [mm], (*P* values)	ReachTime, [ms], (*P* values)	EndAcc, [mm], (*P* values)
SPL_{group}	−36, −49, 57	−12.9 ± 10.3	−0.4 ± 0.6	−4.1 ± 2.8	0.9 ± 0.6
IPS_{indiv}	−42.9, −45.0, 52.9, (±1.9 4.7 4.3)	18.3 ± 13.6	1.0 ± 0.9	−9.2 ± 7.2	**−1.8 ± 0.9, (<0.05)**
SMG_{indiv}	−53.4, −32.5, 40.3, (±8.3 7.5 5.2)	**22.4 ± 8.6, (<0.05)**	0.9 ± 0.3	**12.4 ± 6.2, (0.05)**	0.0 ± 0.8

Note: The MNI coordinates upon which the TMS stimulation sites were planned are given and for TpPath25, MaxDev, ReachTime, and EndAcc, the difference ± SE between trials with versus without TMS is given for each TMS stimulation site—the data of both TMS SOAs is collapsed. Statistically significant differences are marked bold.

Table 3
Results for TMS experiment 3 (HD)

Stimulation Site	MNI coordinates, *x*, *y*, *z* in [mm], (±SD)	TpPath25, [ms], (*P* values)	MaxDev, [mm], (*P* values)	ReachTime, [ms], (*P* values)	EndAcc, [mm], (*P* values)
SPL_{group}	−36, −49, 57	1.9 ± 7.4	0.2 ± 0.3	5.0 ± 10.3	0.3 ± 0.5
$IPS_{HDgroup}$	−39, −45, 50	**15.2 ± 6.3, (<0.05)**	1.2 ± 0.4	21.2 ± 9.1	0.1 ± 0.4
SMG_{group}	−45, −40, 45	**26.8 ± 5.6, (<0.001)**	0.5 ± 0.6	**33.2 ± 5.6, (<0.01)**	0.1 ± 0.3
$SMG_{HDindiv}$	−48.2, −34.2, 38.5, (±8.3 6.3 7.0)	**16.3 ± 10.8, (<0.05)**	−0.2 ± 0.4	**31.3 ± 12.3, (<0.01)**	0.5 ± 0.7
$IPS_{HDright}$	45, −39, 52	1.0 ± 10.0	0.2 ± 0.7	11.4 ± 8.8	0.6 ± 0.6
Reach	−33, −56, 55	1.2 ± 6.5	−0.2 ± 0.5	13.6 ± 8.5	0.7 ± 0.3

Note: The MNI coordinates upon which the TMS stimulation sites were planned are given and for TpPath25, MaxDev, ReachTime, and EndAcc, the difference ± SE between trials with versus without TMS is given for each TMS stimulation site. Statistically significant differences are marked bold. For ReachTime, the interaction TMS × stimulation site did not reach significance. Newman–Keuls rather than Fisher least significant difference was therefore used for multiple comparisons correction in this case.

Table 4
Average absolute values across stimulation sites for all experiments

		TpPath25 [ms]	MaxDev [mm]	ReachTime [ms]	EndAcc [mm]	PeakAcc [cm/s^2]	Time2peakAcc [ms]
Exp. 1: TD_HF	TMS	404 ± 21	12.5 ± 0.9	669 ± 26	0.8 ± 0.5	642 ± 95	182 ± 11
	No TMS	397 ± 20	12.2 ± 1.0	653 ± 26	0.5 ± 0.4	643 ± 95	181 ± 9
Exp. 2: TD_nHF	TMS 40	398 ± 22	20.1 ± 2.0	654 ± 27	−0.1 ± 2.3	771 ± 74	174 ± 8
	TMS 80	403 ± 25	20.9 ± 2.0	659 ± 30	−1.8 ± 2.4	805 ± 83	179 ± 9
	No TMS	391 ± 20	20.0 ± 2.0	658 ± 28	−0.3 ± 2.1	779 ± 71	176 ± 10
Exp. 3: HD	TMS	476 ± 26	19.4 ± 1.0	718 ± 35	−1.1 ± 0.6	709 ± 84	177 ± 12
	No TMS	466 ± 22	19.1 ± 1.1	699 ± 32	−1.5 ± 0.7	727 ± 80	176 ± 13

Note: TpPath25, MaxDev, ReachTime, EndAcc, PeakAcc, and Time2peakAcc are listed separately for trials with TMS (for experiment 2 also separately the TMS SOAs) and without TMS, respectively. The mean ± SE across subjects is given. Positive values of EndAcc represent overcompensation for the perturbation, negative values represent incomplete compensation.

TMS (main effect of TMS: $P > 0.05$) nor did it depend on the stimulation site (Table 3; interaction TMS × stimulation site: $P > 0.9$). TMS over $IPS_{HDgroup}$, SMG_{group}, and $SMG_{HDindiv}$ selectively delayed the onset of the correction to the perturbation (TpPath25 in Table 3; interaction TMS × stimulation site: $F_{5,40} = 2.48$; $P < 0.05$). Maximum deviation (MaxDev in Table 3) was not affected by TMS when correcting for multiple comparisons. The apparent large TMS effect for $IPS_{HDgroup}$ stimulation manifested as trend ($P = 0.02$ uncorrected; paired *t*-test).

Correlations between TMS Effects and fMRI Activation

For both conditions with visual feedback about the hand position (TMS experiments 1 and 3), we tested whether the size of TMS effects correlated with the individual fMRI activation strengths across the different stimulation sites (Fig. 3). A condition corresponding to TD_nHF was not tested in the fMRI experiment and could therefore not be used for a correlation analysis. For every stimulation site, the individual fMRI effect strength was determined in each subject as the mean *Z* value of the corresponding fMRI contrast in a cylindrical mask with radius 5 mm and height 3 cm beneath the TMS coil center. Subsequently, we tested whether the individual TMS effect, as assessed by TpPath25 and MaxDev, correlated with the fMRI effect strength across sites and subjects. The TMS and fMRI effects were ranked across all stimulation sites in each subject in order to prevent that absolute differences between

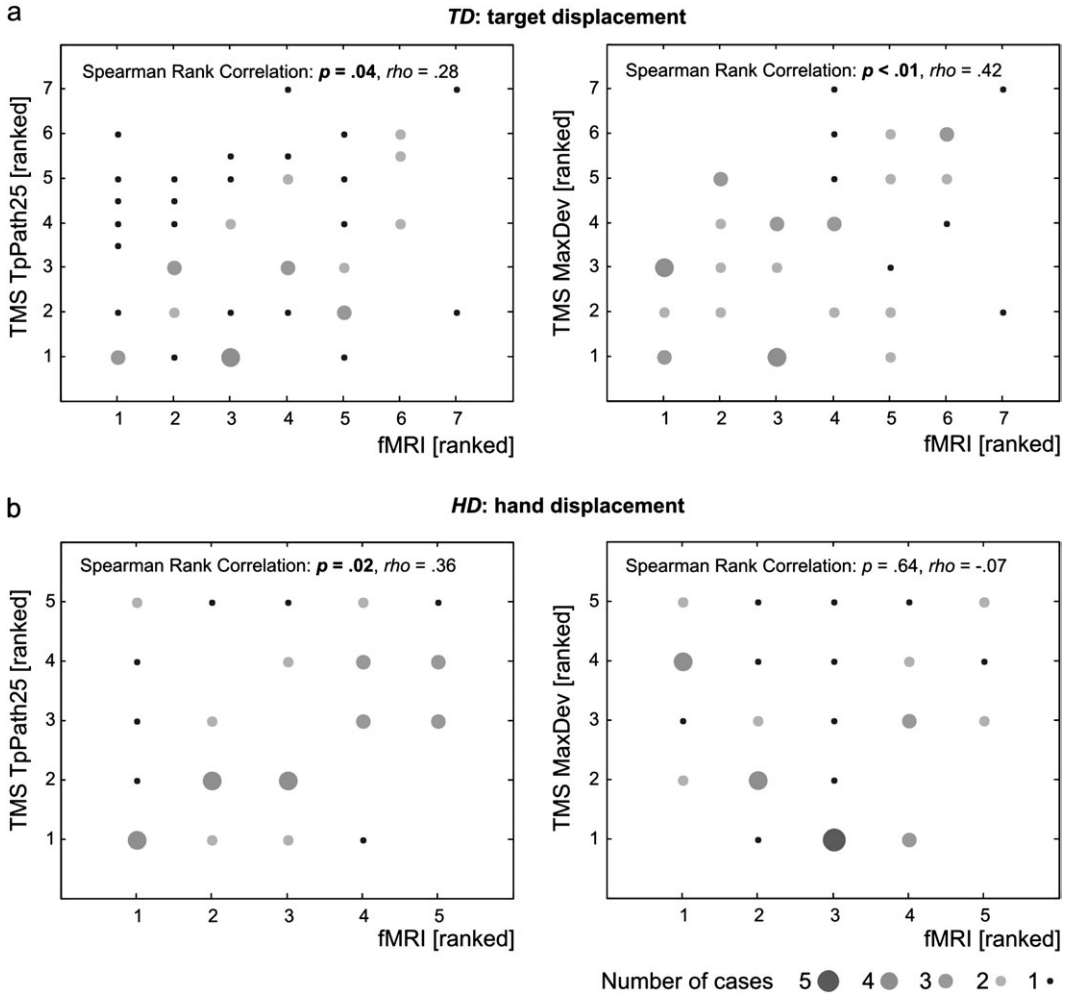

Figure 3. Correlations between ranked fMRI and TMS effects. In the left panels, the TMS effect is measured with TpPath25 on the right panels with MaxDev. (*a*) Correlations for the displacement of the visual target (TD, TMS experiment 1). (*b*) Correlations for the displacement of the visual feedback of the hand position (HD, TMS experiment 3).

subjects, both in BOLD activation and for the TMS measurements, affected the results. Subsequently, Spearman rank correlation tests were conducted on the ranked data across subjects. For TD_HF, both TMS measures were significantly correlated with the fMRI effect (Fig. 3*a*; $P < 0.05$, $\rho = 0.28$ for TpPath25; $P < 0.01$, $\rho = 0.42$ for MaxDev). For HD, TpPath25 correlated well with the fMRI effect (Fig. 3*b*; $P < 0.05$, $\rho = 0.36$). *MaxDev* did not show any correlation (Fig. 3*b*; $P = 0.64$; $\rho = -0.07$), just as this measurement did not reveal strong effects for TMS stimulation as well.

Discussion

We have demonstrated that TMS applied over the anterior IPS (aIPS) and aSMG, but not over other sites on the PPC, reduced the subjects' ability to correct for visual perturbations during reaching movements. This was clear for perturbations of both external and body-related visual information (TMS experiments 1 and 3). Additionally, the cortical sites exhibiting TMS effects remained the same when visual feedback about the hand position was absent (TMS experiment 2). Taken together, our results provide the first causal demonstration that the human aIPS and aSMG are engaged in the integration of sensory information for online control of reaching, independent of the nature of the visual perturbation.

Our results provide support for the existence of 2 distinct, but neighboring parietal regions (aIPS and aSMG): First, the TMS effects consistently occurred over positions that exhibited specific BOLD activity increases for perturbed versus unperturbed reaching in the fMRI experiment. The correlations between fMRI and TMS results support the hypothesis of 2 distinct regions, even though this alone is not sufficient evidence. Second, in TMS experiment 1, the effects at site SMG_{group} were very weak, while a stable impact of TMS occurred at the more inferior position SMG_{indiv}. That is, moving the SMG site further away from the aIPS stabilized (rather than attenuated) the TMS effects. Third, in TMS experiment 2, stimulation over aIPS and SMG_{indiv} yielded opposite behavioral effects: impact on reaching accuracy versus timing of the corrective movement. Fourth, in all experiments, TMS effects were observed at the aIPS and SMG_{indiv} with an average distance of ~20 mm. In contrast, sites closer to the aIPS (SPL, reach, and Desmurget; average distance ~12 mm to the aIPS sites) consistently lacked any effect. Taken together, these findings suggest 2 distinct target sites during the experiments with visual TDs. TMS experiment 3 is less conclusive in this respect as site SMG_{group} between $IPS_{HDgroup}$ and SMG_{indiv} also showed strong effects, and the effects were similar across all 3 sites. However, the consistent spatial pattern found in all

experiments (including the fMRI localizer) at least supports different anatomical sites also for TMS experiment 3. It should be noted that similar spatial resolutions of TMS have previously been observed, for example, in motormapping studies investing the separation between muscle representations (Wilson et al. 1993; Krings et al. 1998), visual suppression studies with 7-mm grids (Thielscher et al. 2010), studies investigating the dependence of phosphenes on coil position (Cowey 2005), and TMS hunting procedures to localize PPC target sites (Ashbridge et al. 1997). Clearly, TMS experiments generally do not qualify for drawing conclusions about the 3D position of the stimulated anatomical location. TMS solely provides a 2D focus and always yields in stronger electric fields in more superficial areas, even when they are not perfectly beneath the center of the coil. However, a rigorous design as pursued in this study provides additional information to control for this problem: Demonstrating that optimal stimulation of adjacent, more superficial sites does not result in behavioral impairment helps to rule out that the TMS effect was caused by disruption of these areas rather than the targeted area. In addition, the distances between the fMRI peak activations and the TMS coil were not significantly different between sites SPL and aIPS/aSMG (data not shown).

Using individually adjusted stimulation intensities, we excluded that TMS caused direct motor impairments that would have biased our results. This was confirmed by the absence of TMS effects when stimulating over the anterior SPL (aSPL), which had a similar distance to the motor cortex (M1) as the sites over the aIPS and aSMG. The correlation between the individual TMS and fMRI effect strengths further argues against any direct TMS effects on M1, just as the observation that the initial movement period was unaffected by TMS (Supplementary Data C.1). Likewise, for TMS experiments 1 and 2, putative effects of the magnetic stimuli on corrective eye movements rather than reaching-related activity were carefully ruled out (Supplementary Data C.2 and C.3). The magnetic pulses were applied after the main saccade to the visual target in all 3 TMS experiments. As TMS experiment 3 did not require compensatory saccades, the reported results could not stem from unintended effects on saccadic activity in first place. Finally, also the spatial pattern of the observed TMS effects (impact on the aIPS and aSMG but not on more posterior control sites) argues against putative TMS effects on saccades as a large body of literature shows that more posterior parts of the PPC are involved in saccade processing (Simon et al. 2002; Konen et al. 2004). The TMS studies in this field always tested more posterior positions compared with our sites and offer inconsistent results on whether left PPC TMS does affect saccades processing (Van Donkelaar et al. 2000; Yang and Kapoula 2004).

Desmurget et al. (1999) were the only group to date demonstrating that TMS over the left IPS largely disturbed online corrections in a visually perturbed reaching paradigm. Using the coil positioning method reported in their study, we stimulated sites over the aSPL and did not find any TMS effect. The effects reported here for the neighboring sites aIPS and aSMG are generally weaker, though in the usual range of TMS studies targeting the PPC. However, there are several methodological differences between the studies that might have contributed to the different results (e.g., spatial extent of the magnetic field induced by the coil, direction of eye movements, and restriction of movement). Importantly, in contrast to their coil positioning strategy which did not take into account interindividual differences in (functional) anatomy, our usage of several stimulation sites allows for a spatially specific mapping to neuroanatomy in respect to the cortical surface. Furthermore, testing different perturbation paradigms enabled us to functionally disentangle the identified regions.

Due to the specificity of area aIPS for actions related to grasping objects that was found in some studies (Binkofski et al. 1998; Tunik et al. 2005; Culham et al. 2006; Rice et al. 2006), this area is commonly regarded as a likely candidate for the human homologue to the macaque's anterior intraparietal area, where neurons respond selectively to hand manipulation tasks (Sakata et al. 1995). Apart from grasping studies, the involvement of area aIPS has also been demonstrated in reaching tasks, both with and without vision of the hand (Desmurget et al. 2001; Filimon et al. 2007, 2009; Taubert et al. 2010). Tunik et al. (2007) recently suggested that the aIPS is more generally involved in online control of motor actions, independent of the effectors that they demonstrated for finger position and wrist orientation in grasping. Our results support this hypothesis by providing direct evidence that it also applies to the hand positioning for reaching, as demonstrated for both external and body-related visual information. For displacement of the visual target without visual feedback about the hand position, TMS over the aIPS significantly impaired the end accuracy of reaching. This suggests that TMS induced relatively long-lasting effects in this specific task that required intact coordinate transformations between the external visual and the body-related proprioceptive information to be continuously maintained throughout the reaching movement. Anatomically, area aIPS is part of the ventro-dorsal stream (Tanne-Gariepy et al. 2002; Rizzolatti and Matelli 2003; Verhagen et al. 2008) and highly interconnected with the ventral premotor cortex (Tomassini et al. 2007). This fronto-parietal circuit is associated with transformations of spatial object locations in motor commands and the adaptation of motor behavior to current conditions by integrating visual information from the ventral stream. This further supports a role of the aIPS in "dynamic, goal-based, sensorimotor transformations" as suggested by Tunik et al. (2007), in addition to the more short-termed TMS effects over the aIPS with visual feedback of the hand position.

Area aSMG has been mainly associated with tasks relying on the integration of visual and proprioceptive/somatosensory information such as hand-object interactions, grasping (Nickel and Seitz 2005; Naito and Ehrsson 2006), and tool use (Johnson-Frey 2004). Fewer studies demonstrated a role of the SMG in reaching (Diedrichsen et al. 2005; Filimon et al. 2007). Diedrichsen et al. (2005) showed that parts of the aSMG exhibited enhanced BOLD activity during the processing of execution errors stemming from miscalibrated internal models of body effectors (e.g., visual-proprioceptive mismatch or altered limb dynamics). Thus, the aSMG might contribute to maintaining coherent representations of body effectors, including resolving discrepancies between expected and actual states. Consistently, in our study, displacement of the visual hand representation created a visual-proprioceptive conflict and TMS disturbance of the aSMG might have delayed the resolution of this conflict, thus causing later online corrections. Alternatively, aSMG stimulation might have interfered with bottom-up proprioceptive information, which is conceptually distinct from disturbing

visual–somatosensory interactions. However, this would rather lead to an attenuation of the visual-proprioceptive conflict and thus a reverse result pattern. Additionally, visual-plus-somatosensory areas were found near the SMG (Bremmer et al. 2001). Unlike Diedrichsen et al. (2005), we found that the aSMG also contributed to the online corrections for displacements of the visual targets. This discrepancy might stem from methodological differences such as different workspaces, or the restriction to fMRI group results versus the assessment of interindividual differences in the aSMG activations. Importantly, our TMS experiments confirmed the causal contribution of aSMG for the correction to all visual perturbations that we tested within the individual subject.

The enhanced BOLD activity for perturbed versus unperturbed reaching extended into the SPL. General reaching (versus fixation) induced activations extending even more medially and posteriorly in the PPC. Even though saccades might have contributed to the more posterior SPL activations in the latter case (Simon et al. 2002), this is consistent with the common view that the SPL is involved in the planning and control of reaching (Nickel and Seitz 2005; Culham et al. 2006; Blangero et al. 2009; Chib et al. 2009). Using fMRI and a joystick task adapted from macaque studies investigating the role of the PPC in visuomotor coordinate transformations (Eskandar and Assad 1999, 2002), Grefkes et al. (2004) suggested the medial parts of the SPL and IPS to be the putative human homologues to the macaque medial intraparietal area, which is part of the parietal reach region. Anatomically, the SPL is part of the dorso-dorsal stream (Tanne-Gariepy et al. 2002; Rizzolatti and Matelli 2003; Verhagen et al. 2008) and highly interconnected with the dorsal premotor cortex (Tomassini et al. 2007). This fronto-parietal circuit is associated with the involvement in non-standard stimulus response mappings, online control of actions, and the processing of visuospatial parameters for grasping irrespective of the viewing conditions (please see Filimon (2010) for a comprehensive review also covering the relation between human and macaque data). Interestingly, in our case, the absence of TMS effects above the SPL indicates that this area might be more important for planning (Vesia et al. 2008) than for online control. An alternative explanation could be that areas contributing to the planning of reaching movements are more superficial in the SPL than areas involved in online control so that planning processes could be more easily disturbed by TMS (Vesia et al. 2008). Regarding the differences in TMS results in this study between SPL and aIPS/aSMG despite similar distances between the fMRI peak activations and the TMS coil (as already mentioned above) argues against this. Furthermore, a recent fMRI study pointed out that the use of finger pointing (as used in some fMRI studies in this field) rather than normal reaching likely shifted the activations more laterally in prior studies (Filimon et al. 2009). Both our fMRI and TMS results indicate more lateral regions when comparing perturbed versus unperturbed reaching but not for general reaching. Thus, the differences between their and our results likely stem from comparing online control versus reaching in general, especially our TMS experiments demonstrate a specific interference during the execution phase.

A number of studies report posterior parts of the PPC close to the parieto-occipital junction being involved in reaching (Diedrichsen et al. 2005; Karnath and Perenin 2005; Culham et al. 2008). The use of simplified finger "reaching" without arm transport (Culham et al. 2008) during fMRI is the likely cause of why we missed these areas. It should be noted, however, that the usage of finger "reaching" during fMRI does not confound the results for the areas that we actually do report (aIPS and aSMG), as TMS confirmed their involvement in fully fledged reaching movements. In fact, our study strengthens the view that these areas are involved in online control of movements rather independent of the body effectors (hand for grasping, arms for reaching, and fingers for "finger-reaching" or pointing), for example, to fine-tune movements in general.

To conclude, using a combination of fMRI localizer task followed by TMS experiments, we demonstrated for the first time a causal contribution of the aIPS and the aSMG to online control of reaching. This underpins the hypothesis that a large network forms the human functional equivalent to the macaque's network of "parietal reach regions" and that this network extends even further inferior than previously thought. Furthermore, we demonstrated that accounting for interindividual differences when investigating the human PPC can reveal the involvement of subregions that are otherwise missed on the group level and that deriving TMS stimulation sites based on individual functional neuroanatomy is a more effective approach than other selection of stimulation sites. In future, this approach can be used to further disentangle the PPC subregions integrating different sensory modalities in reaching and grasping. fMRI allows to localize putative key areas with high spatial resolution, while subsequent individualized TMS can be used to confirm their causal contribution to the task under study.

Supplementary Material

Supplementary material can be found at: http://www.cercor.oxfordjournals.org/.

Funding

This work was supported by a PhD stipend from the Max Planck Society and by the WCU (World Class University) program through the National Research Foundation of Korea funded by the Ministry of Education, Science and Technology (R31-2008-000-10008-0).

Notes

The authors would like to thank Marc Himmelbach for fruitful discussion about the manuscript and Sonja Cornelsen for help in data acquisition. The comments of the anonymous reviewers helped to improve the quality of the paper. *Conflict of Interest*: None declared.

References

Ashbridge E, Walsh V, Cowey A. 1997. Temporal aspects of visual search studied by transcranial magnetic stimulation. Neuropsychologia. 35:1121–1131.

Binkofski F, Dohle C, Posse S, Stephan KM, Hefter H, Seitz RJ, Freund HJ. 1998. Human anterior intraparietal area subserves prehension: a combined lesion and functional MRI activation study. Neurology. 50:1253–1259.

Blangero A, Menz MM, McNamara A, Binkofski F. 2009. Parietal modules for reaching. Neuropsychologia. 47:1500–1507.

Bremmer F, Schlack A, Shah NJ, Zafiris O, Kubischik M, Hoffmann K, Zilles K, Fink GR. 2001. Polymodal motion processing in posterior parietal and premotor cortex: a human fMRI study strongly implies equivalencies between humans and monkeys. Neuron. 29:287–296.

Buss M, Schmidt G. 1999. Control problems in multimodal telepresence systems. In: Frank P, editor. Advances in control, highlights of ECC '99. London: Springer-Verlag. p. 65–101.
Chib VS, Krutky MA, Lynch KM, Mussa-Ivaldi FA. 2009. The separate neural control of hand movements and contact forces. J Neurosci. 29:3939–3947.
Cowey A. 2005. The Ferrier Lecture 2004: what can transcranial magnetic stimulation tell us about how the brain works? Philos Trans R Soc B Biol Sci. 360:1185–1205.
Culham JC, Cavina-Pratesi C, Singhal A. 2006. The role of parietal cortex in visuomotor control: what have we learned from neuroimaging? Neuropsychologia. 44:2668–2684.
Culham JC, Gallivan J, Cavina-Pratesi C, Quinlan DJ. 2008. fMRI investigations of reaching and ego space in human superior parieto-occipital cortex. In: Klatzky R, McWhinney B, Behrmann M, editors. Embodiment, ego-space and action. New York: Psychology Press. p. 247–274.
Culham JC, Kanwisher NG. 2001. Neuroimaging of cognitive functions in human parietal cortex. Curr Opin Neurobiol. 11:157–163.
Culham JC, Valyear KF. 2006. Human parietal cortex in action. Curr Opin Neurobiol. 16:205–212.
Desmurget M, Epstein CM, Turner RS, Prablanc C, Alexander GE, Grafton ST. 1999. Role of the posterior parietal cortex in updating reaching movements to a visual target. Nat Neurosci. 2:563–567.
Desmurget M, Grafton S. 2000. Forward modeling allows feedback control for fast reaching movements. Trends Cogn Sci. 4:423–431.
Desmurget M, Grea H, Grethe JS, Prablanc C, Alexander GE, Grafton ST. 2001. Functional anatomy of nonvisual feedback loops during reaching: a positron emission tomography study. J Neurosci. 21:2919–2928.
Diedrichsen J, Hashambhoy Y, Rane T, Shadmehr R. 2005. Neural correlates of reach errors. J Neurosci. 25:9919–9931.
Eskandar EN, Assad JA. 1999. Dissociation of visual, motor and predictive signals in parietal cortex during visual guidance. Nat Neurosci. 2:88–93.
Eskandar EN, Assad JA. 2002. Distinct nature of directional signals among parietal cortical areas during visual guidance. J Neurophysiol. 88:1777–1790.
Filimon F. 2010. Human cortical control of hand movements: parietofrontal networks for reaching, grasping, and pointing. Neuroscientist. 16:388–407.
Filimon F, Nelson JD, Hagler DJ, Sereno MI. 2007. Human cortical representations for reaching: mirror neurons for execution, observation, and imagery. Neuroimage. 37:1315–1328.
Filimon F, Nelson JD, Huang RS, Sereno MI. 2009. Multiple parietal reach regions in humans: cortical representations for visual and proprioceptive feedback during on-line reaching. J Neurosci. 29:2961–2971.
Grefkes C, Fink GR. 2005. The functional organization of the intraparietal sulcus in humans and monkeys. J Anat. 207:3–17.
Grefkes C, Ritzl A, Zilles K, Fink GR. 2004. Human medial intraparietal cortex subserves visuomotor coordinate transformation. Neuroimage. 23:1494–1506.
Iacoboni M. 2006. Visuo-motor integration and control in the human posterior parietal cortex: evidence from TMS and fMRI. Neuropsychologia. 44:2691–2699.
Johnson H, Haggard P. 2005. Motor awareness without perceptual awareness. Neuropsychologia. 43:227–237.
Johnson-Frey SH. 2004. The neural bases of complex tool use in humans. Trends Cogn Sci. 8:71–78.
Kammer T, Vorwerg M, Herrnberger B. 2007. Anisotropy in the visual cortex investigated by neuronavigated transcranial magnetic stimulation. NeuroImage. 36:313–321.
Karnath HO, Perenin MT. 2005. Cortical control of visually guided reaching: evidence from patients with optic ataxia. Cereb Cortex. 15:1561–1569.
Konen CS, Kleiser R, Wittsack HJ, Bremmer F, Seitz RJ. 2004. The encoding of saccadic eye movements within human posterior parietal cortex. Neuroimage. 22:304–314.
Krakauer JW, Ghilardi MF, Ghez C. 1999. Independent learning of internal models for kinematic and dynamic control of reaching. Nat Neurosci. 2:1026–1031.
Krings T, Naujokat C, Graf v. Keyserlingk D. 1998. Representation of cortical motor function as revealed by stereotactic transcranial magnetic stimulation. Electroencephalogr Clin Neurophysiol. 109:85–93.
Naito E, Ehrsson HH. 2006. Somatic sensation of hand-object interactive movement is associated with activity in the left inferior parietal cortex. J Neurosci. 26:3783–3790.
Nickel J, Seitz RJ. 2005. Functional clusters in the human parietal cortex as revealed by an observer-independent meta-analysis of functional activation studies. Anat Embryol (Berl). 210:463–472.
Pisella L, Grea H, Tilikete C, Vighetto A, Desmurget M, Rode G, Boisson D, Rossetti Y. 2000. An 'automatic pilot' for the hand in human posterior parietal cortex: toward reinterpreting optic ataxia. Nat Neurosci. 3:729–736.
Prablanc C, Martin O. 1992. Automatic control during hand reaching at undetected two-dimensional target displacements. J Neurophysiol. 67:455–469.
Reichenbach A, Thielscher A, Peer A, Bülthoff HH, Bresciani JP. 2009. Seeing the hand while reaching speeds up on-line responses to a sudden change in target position. J Physiol. 587:4605–4616.
Rice NJ, Tunik E, Grafton ST. 2006. The anterior intraparietal sulcus mediates grasp execution, independent of requirement to update: new insights from transcranial magnetic stimulation. J Neurosci. 26:8176–8182.
Rizzolatti G, Matelli M. 2003. Two different streams form the dorsal visual system: anatomy and functions. Exp Brain Res. 153:146–157.
Sakata H, Taira M, Murata A, Mine S. 1995. Neural mechanisms of visual guidance of hand action in the parietal cortex of the monkey. Cereb Cortex. 5:429–438.
Sarlegna F, Blouin J, Bresciani JP, Bourdin C, Vercher JL, Gauthier GM. 2003. Target and hand position information in the online control of goal-directed arm movements. Exp Brain Res. 151:524–535.
Sarlegna F, Blouin J, Vercher JL, Bresciani JP, Bourdin C, Gauthier GM. 2004. Online control of the direction of rapid reaching movements. Exp Brain Res. 157:468–471.
Simon O, Mangin JF, Cohen L, Le Bihan D, Dehaene S. 2002. Topographical layout of hand, eye, calculation, and language-related areas in the human parietal lobe. Neuron. 33:475–487.
Tanne-Gariepy J, Rouiller EM, Boussaoud D. 2002. Parietal inputs to dorsal versus ventral premotor areas in the macaque monkey: evidence for largely segregated visuomotor pathways. Exp Brain Res. 145:91–103.
Taubert M, Dafotakis M, Sparing R, Eickhoff S, Leuchte S, Fink GR, Nowak DA. 2010. Inhibition of the anterior intraparietal area and the dorsal premotor cortex interfere with arbitrary visuo-motor mapping. Clin Neurophysiol. 121:408–413.
Thielscher A, Reichenbach A, Ugurbil K, Uludag K. 2010. The cortical site of visual suppression by transcranial magnetic stimulation. Cereb Cortex. 20:328–338.
Tomassini V, Jbabdi S, Klein JC, Behrens TE, Pozzilli C, Matthews PM, Rushworth MF, Johansen-Berg H. 2007. Diffusion-weighted imaging tractography-based parcellation of the human lateral premotor cortex identifies dorsal and ventral subregions with anatomical and functional specializations. J Neurosci. 27:10259–10269.
Tunik E, Frey SH, Grafton ST. 2005. Virtual lesions of the anterior intraparietal area disrupt goal-dependent on-line adjustments of grasp. Nat Neurosci. 8:505–511.
Tunik E, Rice NJ, Hamilton A, Grafton ST. 2007. Beyond grasping: representation of action in human anterior intraparietal sulcus. Neuroimage. 36(Suppl 2):T77–T86.
Van Donkelaar P, Lee JH, Drew AS. 2000. Transcranial magnetic stimulation disrupts eye-hand interactions in the posterior parietal cortex. J Neurophysiol. 84:1677–1680.
Verhagen L, Dijkerman HC, Grol MJ, Toni I. 2008. Perceptuo-motor interactions during prehension movements. J Neurosci. 28:4726–4735.
Vesia M, Yan X, Henriques DY, Sergio LE, Crawford JD. 2008. Transcranial magnetic stimulation over human dorsal-lateral

posterior parietal cortex disrupts integration of hand position signals into the reach plan. J Neurophysiol. 100:2005–2014.
Wilson SA, Thickbroom GW, Mastaglia FL. 1993. Transcranial magnetic stimulation mapping of the motor cortex in normal subjects. The representation of two intrinsic hand muscles. J Neurol Sci. 118:134–144.
Yang Q, Kapoula Z. 2004. TMS over the left posterior parietal cortex prolongs latency of contralateral saccades and convergence. Invest Ophthalmol Vis Sci. 45:2231–2239.
Zuber BL, Stark L. 1966. Saccadic suppression: elevation of visual threshold associated with saccadic eye movements. Exp Neurol. 16:65–79.

Reichenbach et al.

Contributions of the PPC to online control of visually guided reaching movements assessed with fMRI-guided TMS

Supplementary Data

A. TMS Experiments: Setup and Exemplary Data

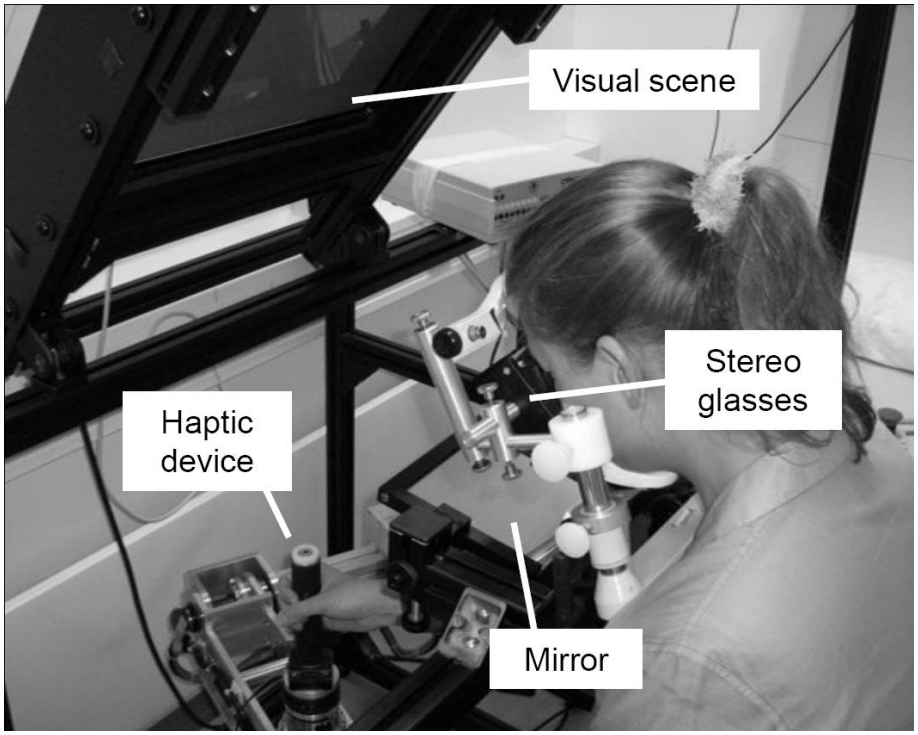

Figure S1 Experimental VR setup for the TMS experiments. During the experiments, an additional black cloth in the horizontal plane between the mirror and the robot arm prevented the subjects to get visual feedback about their real hand movement.

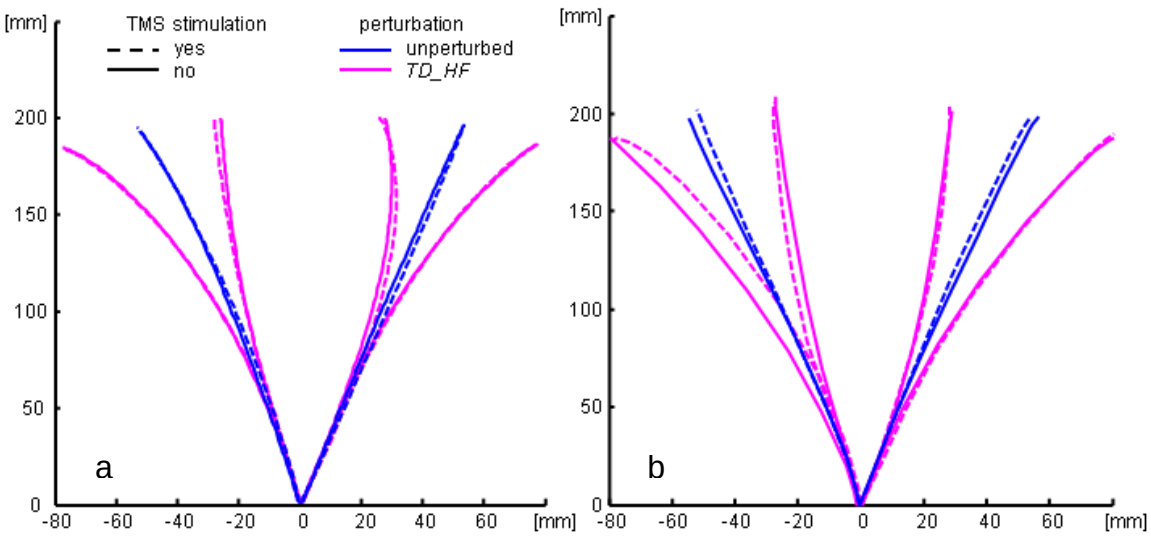

Figure S2 Additional behavioral data for TMS experiment 1. Shown are exemplary 2D trajectories for site IPS_{group} (equivalent to Fig. 1c), averaged across subjects (a) and for an exemplary single subject (b). The trajectories are aligned to the starting position and normalized over time.

B. fMRI Localizer Experiment

B.1 Stimuli and Behavioural Task

Stimuli were presented using Cogent 2000 (University College London, UK), projected on a screen located 100 cm away from the subject's eyes (LCD projector JVC DLA-SX21) and viewed through a coil-mounted mirror. The size of the visual scene was matched to the visual scene of the TMS experiments in terms of viewing angle. The subject's right index finger was fixated on the top of a MR-compatible joystick placed beside the hip (Current Designs, Inc., Philadelphia, USA), allowing a workspace of about

4x4 cm. The right wrist and arm rested comfortably on a pillow, thereby preventing motion artifacts.

The session comprised 7 runs of about 10 min each, including an initial training run without acquisition of MR images. One run consisted of 9 blocks presented in a counter-balanced order: 4 reaching blocks (70-90 s each, dependent on subject's reaching time), and 5 fixation blocks (~30 s each). Each block was preceded by a screen informing the subject about the actual task. The reaching blocks contained 10 trials in which the subject had to move the eyes and the joystick cursor (represented by a red circle) from the starting circle to the target circle (both represented by a magenta circle) as quickly and precisely as possible. A fast event-related design was used to assess the effects of the different visual perturbations within different trials. Four trial types occurred with equal probability in a pseudo randomized order: 1) no perturbation, 2) displacement of the visual target (abbreviated *TD* indicating 'target displacement', Fig. 1a), 3) displacement of the visual feedback about the 'hand' position, i.e. the joystick cursor (abbreviated *HD* indicating 'hand displacement' according to the terminology used in the TMS main experiments, Fig. 1b), or 4) rotation of the visual feedback about the 'hand' position, i.e. the joystick cursor (included in the fMRI analysis but not used as further condition in the TMS experiments in order to limit the complexity and length of the overall study). After reaching for the target, the subjects had to wait motionless for 4 s at the end of each trial until a new starting circle appeared, resulting in an average trial duration of 4.93 (±0.55 SD) s. The displacements occurred at 10% of the way from the starting circle to the target. In the fixation blocks, the starting circle had to be continuously fixated (controlled by online monitoring on the eye-tracking screen (ASL Long Range Optic, Applied

Science Laboratories, Bedford (MA), USA)) and the hand had to be kept still. The visual scene was matched to the unperturbed reaching condition, using pre-recorded trials.

B.2 Imaging Parameters and Data Analysis

Scanning was performed on a Siemens 3T TIM Trio (Siemens, Erlangen, Germany) with a 12 channel head coil. Whole-brain functional images were recorded using gradient echo planar imaging (TR 2580 ms, TE 35 ms, 40 horizontal slices, in-plane resolution 3x3 mm^2, slice thickness 2.5 mm, gap 0.5 mm). Up to 230 volumes were acquired per experimental run, including four initial volumes which were discarded to allow for T1 equilibration. Additionally, a T1-weighted structural image was acquired (MPRAGE, TR 1900 ms, TE 2.26 ms, TI 900 ms, flip angle 9°, 192 coronal slices, 1 mm iso-voxel resolution, 2 averages). The functional data was analyzed using FSL 4.0 (FMRIB, Oxford, UK; (Smith et al. 2004; Smith et al. 2005)). The EPI volumes were motion-corrected, temporally high-pass filtered (100 s cutoff), spatially smoothed (Gaussian with 5 mm FWHM) and registered to the individual structural image using FLIRT (Jenkinson et al. 2002).

First, regions exhibiting robust reaching-related activity were determined. The BOLD activation was modeled as the convolution of the actual timings from the block design pattern with a standard hemodynamic response function (HRF), resulting in two regressors for the different block types (reaching & fixation). For each subject, separate general linear models were estimated for each experimental run and combined on the single-subject level using a fixed-effects analysis. Regions were assessed that showed higher BOLD activity during reaching than during fixation blocks (tested at $Z = 2.3$ voxel level and $p = .05$ corrected at cluster level using Gaussian random field theory (Worsley

et al. 1992)). In order to create group results, the maps of the individual parameter estimates were normalized to MNI space by registering the structural image to the MNI template (Mazziotta et al. 2001) using FLIRT (Jenkinson et al. 2002) with 12 degree-of-freedom linear registration. The normalized individual maps of parameter estimates were fed into a second-level mixed-effects analysis using FLAME (Beckmann et al. 2003) with experimental conditions (reaching vs. fixation) and subjects as fixed and random factors, respectively. Again, regions exhibiting higher activity for reaching compared to fixation were determined ($Z = 2.3$ voxel level and $p = .05$ corrected at cluster level using Gaussian random field theory (Worsley et al. 1992)). For both analyses, on the single-subject and group level, the resulting statistical maps were used as masks in the subsequent analysis to ensure that the observed regions exhibited robust reaching-related activation.

As we were interested in regions involved in online control of reaching, the trials with visual perturbations were compared to unperturbed reaching as next step. The regressor representing the reaching blocks was substituted by four event-related regressors modeling the BOLD signal for the different types of reaching trials. Each of the regressors was created by convolving the time frame pattern of the corresponding reaching trials with a HRF. In two separate analyses, regions were determined that exhibited higher activity in trials with displaced visual target (*TD*) and in trials with displaced visual feedback of the hand position (*HD*), respectively, than in unperturbed trials. The same analysis sequence was applied as described above for the general reaching-related activity.

C. Control Experiments and Analyses

We conducted additional control analyses and experiments to rule out that the results presented in the main part of the paper were affected by a direct motor impairment of the TMS pulses or by an impact of TMS on saccadic- rather than reaching-related activity.

C.1 TMS impact on the initial movement period

As control, we analyzed the initial acceleration period of the reaching movements (Desmurget et al. 1999). The time needed to reach the peak acceleration at the beginning of the movement was around 180 ms, which included the time period during which the TMS stimuli were delivered. Direct TMS effects on the motor cortex (inducing, e.g. muscle twitches and silent periods) have short latencies so that, in our case, general motor impairments by TMS should also affect the initial acceleration period (Desmurget et al. 1999). Therefore, in order to rule out that the observed TMS effects over SMG and IPS were due to general motor impairments, we analyzed the peak acceleration (*PeakAcc*) and the time needed to reach it (*Time2peakAcc*) for all trials with visual perturbations of all three experiments (Table 4). There was neither an effect of the TMS pulses on the peak acceleration (main effect of TMS: $p > .3$; interaction TMS * stimulation site: $p > .2$) nor on the time to reach it (main effect of TMS: $p > .4$; interaction TMS * stimulation site: $p > .3$) for any experiment.

C.2 TMS influence on the corrective saccade

Rationale

To exclude the possibility that the observed TMS effects on reaching movements could stem from a disruption of the corrective saccade to the displaced target – for the experiment with the displaced visual hand feedback no such corrective saccade is necessary – the onset of the corrective saccades was determined using additional experimental recordings.

Experimental Procedure and Task

TMS experiment 1 (*TD_HF*) was repeated for three TMS stimulation sites: Two stimulation sites exhibiting consistent TMS effects (IPS_{group} and SMG_{indiv}), and one site where TMS had no effect on the reaching correction (SPL_{group}). Additionally, the vertical and horizontal components of the eye movements were recorded via electro-oculography (EOG). Two pairs of electrodes were placed above and below the right eye as well as adjacent to the inner and outer corner after cleaning the skin with alcohol. A ground electrode was placed on the subject's forehead. These electrodes were connected to a BrainAmp MR plus amplifier and the signals were converted with BrainVision software (Brain Products, Germany) on a laptop. A custom-made MATLAB (The MathWorks, Natick, Massachusetts, USA) program saved the potentials from both directions (horizontal/vertical) seperately, from 300 msec before until 1000 msec after a trigger indicating the perturbation.

EOG Data Analysis

We assessed the first correction-specific changes of EOG activity after the first saccade (which triggered the perturbation). We focused on the horizontal component of the EOG signal as this component was specific to horizontal target displacements. Within the TMS trials, the window around the TMS pulses was interpolated using a spline function. As the

expected onset of the corrective saccade (Becker and Fuchs 1969) was far beyond this time-window, this did not result in any bias. For each EOG trace, the AC component of the signal was then smoothed using a rectangular sliding window of 50 msec. The EOG latencies were determined using the first derivative of the signal. To define saccade onset, the first derivative of the perturbed trials had to stay for 25 msec above the threshold which was set for each subjects individually. Afterwards, each detected onset was checked manually via visualization of the EOG signal, its first derivative, and the reported onset (Fig. S3). If necessary, it was corrected manually. This procedure resulted in a detection rate of 94% and 91% for trials with and without TMS, respectively.

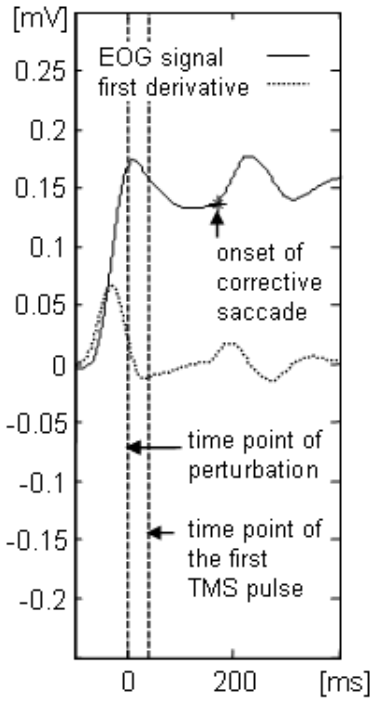

Figure S3 Visualization of the horizontal EOG signal, its first derivative, and the reported onset of the corrective saccade.

As a prior TMS study (Yang and Kapoula 2004) showed effects only on saccades to the right when TMS was administered to the left PPC (with stimulation sites more posterior than the ones tested here), we analyzed the data for all target positions and perturbation directions independently.

Results

Five of the subjects who took part in the main experiment were tested and none of them showed any TMS-evoked disruption of the corrective saccade. The onset of the corrective saccade without TMS stimulation varied between subjects and was in the range between 160 and 205 ms. Neither condition-specific (target location * perturbation direction) nor pooled data analysis revealed any intra-subject effects in favor of a disruption of the corrective saccade by TMS at any stimulation site. Also on the group level (figure S4), no indication for a disruption of the corrective saccade by TMS can be found.

Conclusion

The TMS stimulation did not delay the onset of the corrective saccade for any of the stimulation sites tested. Therefore, the possibility that the observed TMS effect on reaching movements resulted from a disruption of corrective saccades seems very unlikely.

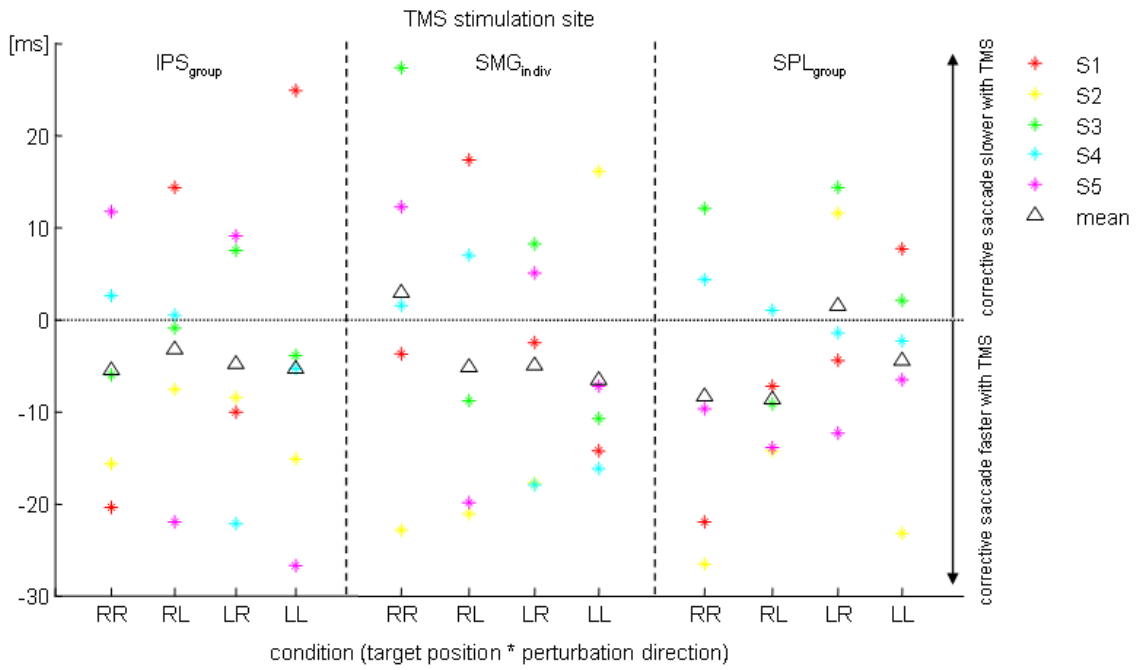

Figure S4 Differences in onset of the corrective saccade (onset with TMS – onset without TMS) for all subjects (S1 – S5, differently colored asterisks) and their mean (black triangle). The three panels depict the data for the three TMS stimulation sites. The data is shown separately for all conditions (target position * perturbation direction) – RR: target to the right, perturbation to the right; RL: target to the right, perturbation to the left; LR: target to the left, perturbation to the right; LL: target to the left, perturbation to the left.

C.3 FMRI activity for reaching + saccades vs. saccades only

Rationale

To exclude the possibility that the enhanced BOLD activity for the perturbed trials was mainly driven by (corrective) saccades, we conducted a control fMRI experiment contrasting BOLD activity during reaching + saccades vs. saccades only, both for perturbed and unperturbed trials.

Experimental Procedure and Task

The fMRI localizer task was repeated with 5 subjects and the following modifications: In the reaching blocks only unperturbed and target displacement trials were used, randomly intermixed. Instead of fixation blocks, we used the visual stimulation of the previous reaching blocks and instructed the subjects to make a saccade to the target, i.e. the very same task as in the reaching block only without the reaching movement.

fMRI Data Analysis

Regions exhibiting larger reaching-related activity (incl. saccades) than only saccade-related activity were determined. The BOLD activation was modeled as the convolution of the block design pattern with a standard hemodynamic response function (HRF), resulting in two regressors for the different block types (reaching & saccades). For each subject, separate general linear models were estimated for each experimental run and combined on the single-subject level using a fixed-effects analysis. Regions were assessed that showed higher BOLD activity during reaching than during saccade blocks (tested at $Z = 2.3$ voxel level and $p = .05$ corrected at cluster level). In order to create group results, the maps of the individual parameter estimates were normalized to MNI space by registering the structural image to the MNI template (Mazziotta et al. 2001). The normalized individual maps of parameter estimates were fed into a second-level mixed-

effects analysis with experimental conditions (reaching vs. saccades) and subjects as fixed and random factors, respectively. Again, regions exhibiting higher activity for reaching compared to saccades were determined (Z = 2.3 voxel level and p = .05 corrected at cluster level).

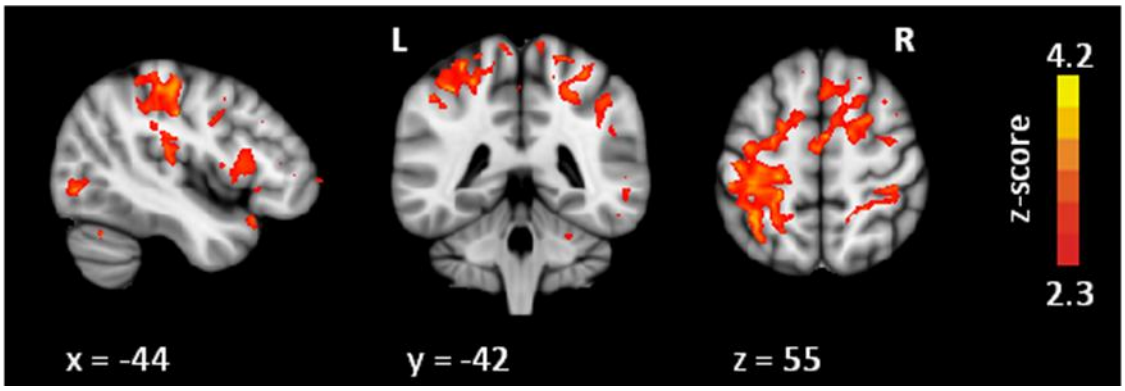

Figure S5 fMRI activation pattern for reaching + saccades vs. saccades only for the group analyses (thresholded at Z = 2.3 voxel level and p = .05 cluster level). The depicted position corresponds to the MNI coordinates of IPS_{group}.

Results

Larger BOLD activity for reaching + saccades vs. saccades only mainly clustered in the left hemisphere (Fig. S5), spanning from motor cortex over somatosensory cortex to the posterior parietal cortex (PPC). Additional activations occurred bilaterally in the frontal lobes (including premotor areas) and the right cerebellum. A smaller cluster was present in the right PPC. All MNI coordinates on which TMS stimulation sites were planned

upon had a *Z*-value > 1.6, i.e. robust larger activation for reaching+saccades vs. saccades only. Site IPS_{group} (depicted in Fig. S5) had a *Z*-value of 2.7.

Conclusion

The brain sites serving as basis for the stimulation sites robustly exhibited stronger BOLD activity for reaching incl. saccades than for saccades alone. Therefore, the possibility that the observed effects of perturbed vs. unperturbed reaching in the original fMRI localizer stemmed predominantly from additional saccadic activity seems very unlikely.

References

Becker W, Fuchs AF. 1969. Further properties of the human saccadic system: eye movements and correction saccades with and without visual fixation points. Vision Res. 9: 1247-1258.

Beckmann CF, Jenkinson M, Smith SM. 2003. General multilevel linear modeling for group analysis in FMRI. Neuroimage. 20: 1052-1063.

Desmurget M, Epstein CM, Turner RS, Prablanc C, Alexander GE, Grafton ST. 1999. Role of the posterior parietal cortex in updating reaching movements to a visual target. Nat Neurosci. 2: 563-567.

Jenkinson M, Bannister P, Brady M, Smith S. 2002. Improved optimization for the robust and accurate linear registration and motion correction of brain images. Neuroimage. 17: 825-841.

Mazziotta J, Toga A, Evans A, Fox P, Lancaster J, Zilles K, Woods R, Paus T, Simpson G, Pike B, Holmes C, Collins L, Thompson P, MacDonald D, Iacoboni M, Schormann T, Amunts K, Palomero-Gallagher N, Geyer S, Parsons L, Narr K, Kabani N, Le Goualher G, Boomsma D, Cannon T, Kawashima R, Mazoyer B. 2001. A probabilistic atlas and reference system for the human brain: International Consortium for Brain Mapping (ICBM). Philos Trans R Soc Lond B Biol Sci. 356: 1293-1322.

Smith SM, Beckmann CF, Ramnani N, Woolrich MW, Bannister PR, Jenkinson M, Matthews PM, McGonigle DJ. 2005. Variability in fMRI: a re-examination of inter-session differences. Hum Brain Mapp. 24: 248-257.

Smith SM, Jenkinson M, Woolrich MW, Beckmann CF, Behrens TE, Johansen-Berg H, Bannister PR, De Luca M, Drobnjak I, Flitney DE, Niazy RK, Saunders J, Vickers J, Zhang Y, De Stefano N, Brady JM, Matthews PM. 2004. Advances in functional and structural MR image analysis and implementation as FSL. Neuroimage. 23 Suppl 1: S208-219.

Worsley KJ, Evans AC, Marrett S, Neelin P. 1992. A three-dimensional statistical analysis for CBF activation studies in human brain. J Cereb Blood Flow Metab. 12: 900-918.

Yang Q, Kapoula Z. 2004. TMS over the left posterior parietal cortex prolongs latency of contralateral saccades and convergence. Invest Ophthalmol Vis Sci. 45: 2231-2239.